2nd CEPHONA Workshop
on Microscopic Characterisation
of Materials and Structures for Photonics

Warsaw, November 22-23, 2004

STRUCTURAL AND ANALYTICAL CHARACTERIZATION OF SEMICONDUCTOR QUANTUM DOTS BY TEM

H. Kirmse, R. Otto, I. Häusler, I. Hähnert, W. Neumann

Humboldt-Universität zu Berlin, Institut für Physik, AG Kristallographie,
Newtonstrasse 15, D-12489 Berlin, Germany.
email of presenting author: holm.kirmse@physik.hu-berlin.de
web: http://crysta.physik.hu-berlin.de

ABSTRACT

In this paper basic principles of methods of transmission electron microscopy are presented. The applicability of the methods is discussed for determination of either structural or chemical peculiarities. Examples of investigations of semiconductor quantum dot structures illustrate the potential use and limits of the individual method.

1. INTRODUCTION

Nanostructured semiconductor materials, particularly quantum structures are of great interest because the dimensionality on the nanometer scale may drastically change the density of electronic states and the optoelectronic properties. The state of the art of growth, characterization and application of self-organized quantum dot (QD) structures is reviewed by Bimberg et al. [1]. The optoelectronic properties of QD devices such as quantum dot lasers are a function of size, shape, arrangement, and chemical composition of the QDs.

For the determination of the structural and chemical properties of nanosized objects like the QDs methods providing a lateral resolution of smaller than 1 nm have to be applied. A very well suited method is transmission electron microscopy (TEM) including all the modes of imaging, diffraction and spectroscopy (cf. Fig. 1) combined in modern TEMs.

Fig. 2 gives a roadmap for choosing the appropriate TEM method for characterizing QD structures with respect to those peculiarities like structure, deformation of the lattice and chemical composition.

For learning more about structural properties comprising size, shape, arrangement of the QDs, and formation of defects the different modes of conventional TEM (CTEM) can be applied (see chapter 3). CTEM includes bright- (BF), dark-field (DF) as well as weak-beam imaging. The latter one is a particular DF technique.

In addition, by means of high-resolution TEM (HRTEM) assisted by image contrast simulations structural information is gained on an atomic scale. The quantitative analysis of HRTEM images (qHRTEM) delivers detailed knowledge about the lattice deformation closely correlated with strain induced formation of the QDs (see chapter 4). The results can be verified by finite element method (FEM) calculation of strain distribution and strain relaxation in TEM specimens.

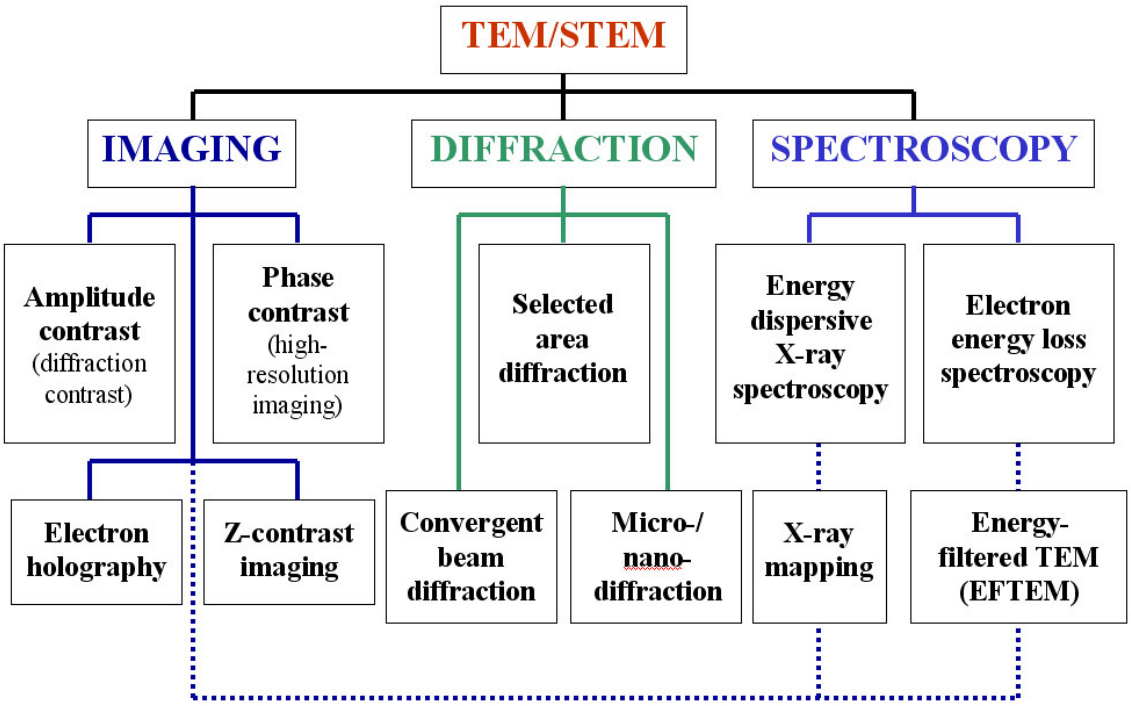

Fig. 1: Overview TEM methods

Beside structural properties the chemical composition of the QDs is one of the most important parameter for the simulation of its electronic and optical properties. The elemental distribution can be two-dimensionally visualized by energy-filtered TEM (EFTEM) and by STEM / Z contrast imaging. Examples for the application to QDs are shown in the chapters 5 and 6. The electron energy loss spectroscopy (EELS) applied to a single QD can deliver qualitative and in special cases also quantitative information on the composition. For chemical characterization HRTEM in combination with image contrast simulations can be used as well. In case of the presence of chemically sensitive reflections (see chapter 3) DF images exhibit image contrast which is sensitive to the distribution of the elements in the region of the QD.

An extensive overview of the various methods is given by Williams and Carter [2].

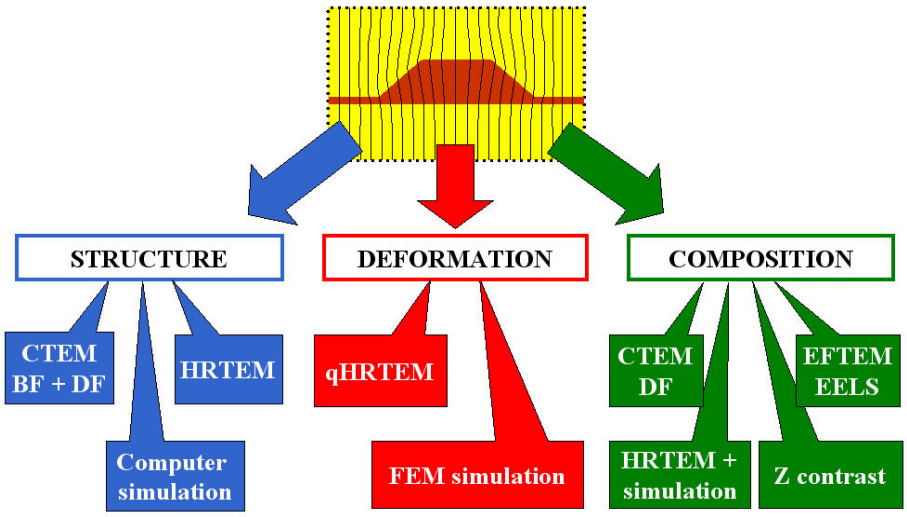

Fig. 2: TEM methods for investigations of QD properties

2. TEM SPECIMEN PREPARATION

The aim of the TEM investigations is to give some statements about the properties of the sample initially grown via, e.g., epitaxial process. With respect to this some restrictions inseparably connected with the TEM method have to be accepted.

The strong interaction between the electrons of the incident beam and the atoms of the specimen requires a sufficiently thin sample. The initial sample has to be thinned by destructive preparation. One has to be aware of preparation artefacts like formation of defects or thin film relaxation when strained materials systems are incorporated in the sample as it is the case for the QD structures. The appropriate specimen thickness is defined by the method which is used for investigation. HRTEM, EELS, EFTEM, and Z contrast require a thickness of only some nanometers. For diffraction contrast imaging the thickness can range from a few 10 nm up to a few 100 nm.

A further restriction is the limited volume which can be analyzed in the TEM. The results obtained at a certain position of the specimen have to be verified by additional measurements at other positions.

In case of epitaxially grown QD structures mainly two projections are favourable for the investigation of their structural and chemical properties namely plan view and cross-sectional view. In plan-view projection the QDs are looked at from the top. Edge-on projection of the QDs is realized in cross-sectional specimens (see Fig. 3).

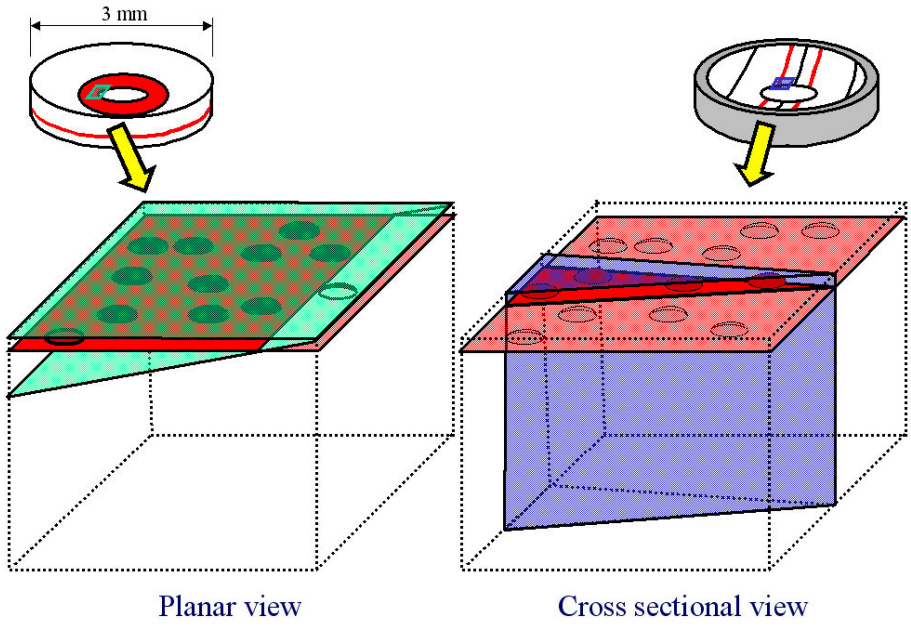

Fig. 3: Correlation between TEM specimen and initial epitaxial sample

The properties of the QDs which can be characterized using either plan-view or cross-sectional samples are summarized in Table 1.

For routine preparation in the Si based semiconductor industry focussed ion beam (FIB) systems are available. These machines enable automatic generation of TEM lamella within a few hours. The resulting lamella has a thickness of about 100 nm including an about 30 nm thick amorphous layer at both sides Those samples are suitable for failure analysis of device structures at a lateral scale of some nanometres.

Numerous strategies of TEM preparation were developed for a more advanced analysis of the specimen on an atomic scale (see, e.g., [3], [4]). Almost all strategies for preparation of semiconductor structures comprise formatting down to a lateral size of 3 mm in diameter, mechanical pre-thinning, dimple grinding and final ion milling down to electron transparency. The benefit of such a sample is the wedge shape of the transparent region providing optimum thickness for the application of different TEM methods discussed in the following chapters.

Property of the QDs	Plan view	Cross section
Area density	✓	—
Lateral arrangement	✓	—
Vertical alignment	—	✓
Lateral size	✓	✓
Vertical size	—	✓
Formation of defects	✓	✓
Presence of a wetting layer	—	✓
Chemical composition	—	✓

Table 1: Capability of plan-view and cross-sectional specimen
for the determination of structural and chemical peculiarities of QDs.

3. DIFFRACTION CONTRAST IMAGING

For crystalline materials the incident electrons undergo a diffraction process. In correspondence to the distance d between the lattice planes and the wavelength λ of the electrons the diffraction angle θ is defined. θ can be derived from Braggs law:

$$\theta = \arcsin\left(\frac{\lambda}{2 \cdot d}\right)$$

The diffraction pattern is formed in the back focal plane of the objective lens (cf. Fig. 4). Applying appropriate excitation of the image forming lenses the diffraction pattern can be projected in the image plane (diffraction mode).

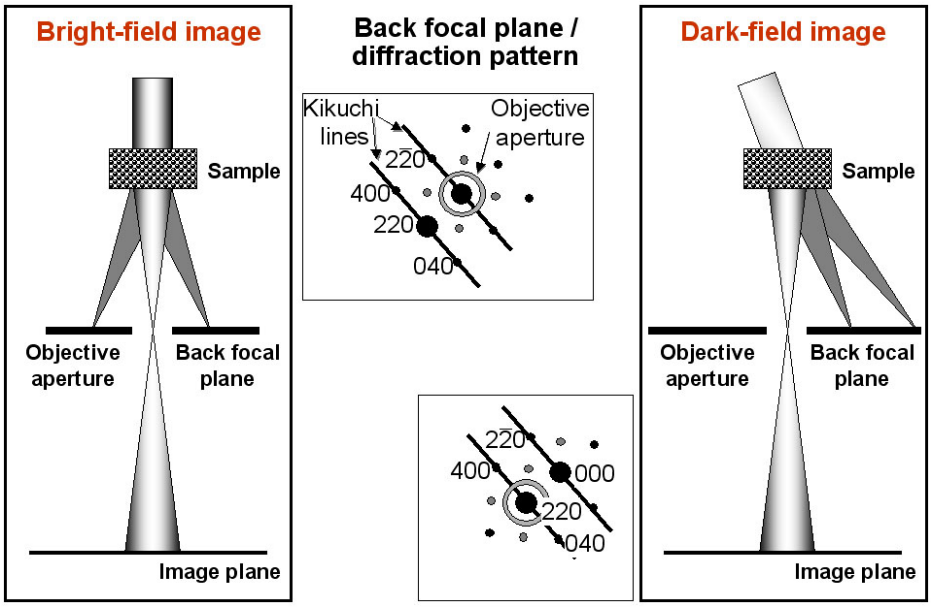

Fig. 4: Diffraction contrast imaging modes and optimum alignment of diffraction pattern

Diffraction contrast imaging utilizes the intensity of an individual beam. Only selecting the non-diffracted beam by the objective aperture a bright-field image is acquired in imaging mode (see left part of Fig. 4). In order to ensure a direct association of the intensity distribution of the BF image with an individual set of lattice planes the two beam case has to be adjusted. This can be realized in diffraction mode by exactly aligning the edges of the Kikuchi band on the non-diffracted and on one diffracted beam (cf. 000 beam and 220 beam in Fig. 4).

The right part of Fig. 4 represents the alignment for dark-field imaging. For this mode the diffracted beam is adjusted on the optical axis of the microscope by tilting the incident electron beam by the diffraction angle. When not tilting the incident beam but simply selecting a diffracted beam passing away from the optical axis the influence of lens aberrations become important and produce artefacts in the image. Hence, the interpretation of the image contrast becomes more complicate.

For the two beam case and for a thin sample, i.e., thickness less than the extinction length, kinematical theory can be applied for describing the interaction between electron and sample material. The intensity of the diffracted beam is defined as:

$$I_{hkl} \propto {F_{hkl}}^2$$

where F_{hkl} is the structure amplitude which can be described as

$$F_{hkl} = \sum_{\nu} f_{\nu} \cdot e^{i \cdot \vec{g} \cdot \vec{r}_{\nu}} .$$

with f_{ν} – atomic scattering amplitude, $\vec{g}$ – diffraction vector and $\vec{r}_{\nu}$ - position of the atom ν.

Most of the semiconducting materials, as, e.g., GaAs, InAs, GaSb, ZnSe, CdSe are crystallizing in the sphalerite structure. For this structure there are two prominent beams 004 and 002. For these the intensity is found to be:

$$I_{004} \propto {F_{004}}^2 = \left\{4 \cdot \left(f_{II/III} + f_{VI/V}\right)\right\}^2 \qquad \text{and} \qquad I_{002} \propto {F_{hkl}}^2 = \left\{4 \cdot \left(f_{II/III} - f_{VI/V}\right)\right\}^2 .$$

The intensity of the 004 beam depends on the sum of both the atomic scattering amplitude f of the group II (or group III) element and that of the group VI (V) element. Thus, 004 dark-field images visualize the strain field. Contrary to that, the intensity of the 002 beam depends on the difference of the f values. Corresponding dark-field images are predominantly chemically sensitive.

Two examples are given below to illustrate the application of diffraction contrast imaging to epitaxially grown semiconductor quantum dot structures.

3.1. CdSe QUANTUM DOTS ON ZnSe

In the cross-sectional diffraction contrast image of Fig. 5 the region of the CdSe layer is visualized. For minimization of contrast contributions caused by preparation artifacts visible in the ZnSe matrix, imaging was done with the 004 diffracted beam strongly excited. The image clearly demonstrates the existence of a wetting layer, appearing as continuous narrow stripe with dark contrast compared to the adjoining ZnSe. Note, that the interfacial zones are almost free of defects. The additional dark contrast phenomena (marked by arrows) with distinctly larger extension into growth direction represent the location of QDs. The contrast of these objects is drastically influenced by strain fields in their surrounding, caused by the large (7 %) ZnSe/CdSe lattice mismatch. Therefore, the TEM bright-field images enable only a rough estimate of the QD cross-section, yielding an average size of about 15 nm in width and 5 nm in height. Weak contrast changes along the wetting layer on a small lateral scale might indicate fluctuations in the strain field as well as in the chemical composition, i.e. alloying during overgrowth [5].

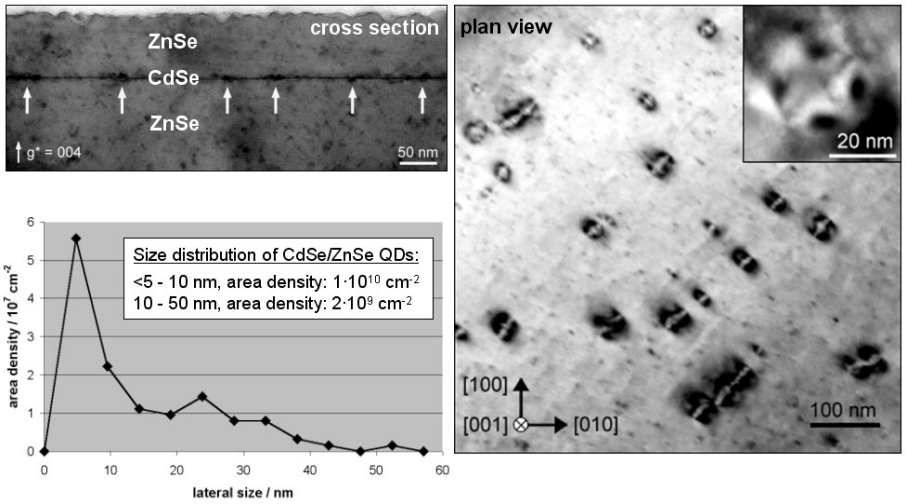

Fig. 5. TEM diffraction contrast imaging of CdSe QDs on ZnSe in cross section and plan view. Size distribution is concluded from plan-view image.

The area distribution and again the lateral size of the ZnSe QDs are determined from TEM plan-view images of the specimen. The right part of Fig. 5 gives an overview revealing QDs of different sizes of their contrast features. The size distribution is presented in the diagram (lower left of Fig. 5). The smaller contrast features show no specific inner contrast according to their small size. Depending on the local orientation some of the larger contrast features show a fourfold symmetry (see inset) which hints to the shape of the QDs. With respect to the lateral alignment of the QDs some cases of alignment parallel to the two ⟨110⟩ directions can be seen.

In order to determine the shape of the QDs the contrast feature in bright-field mode was simulated and compared with experimental findings. In the experimental image a bright four-fold star is visible with its spikes aligned parallel to the ⟨110⟩ directions (cf. Fig. 6a).

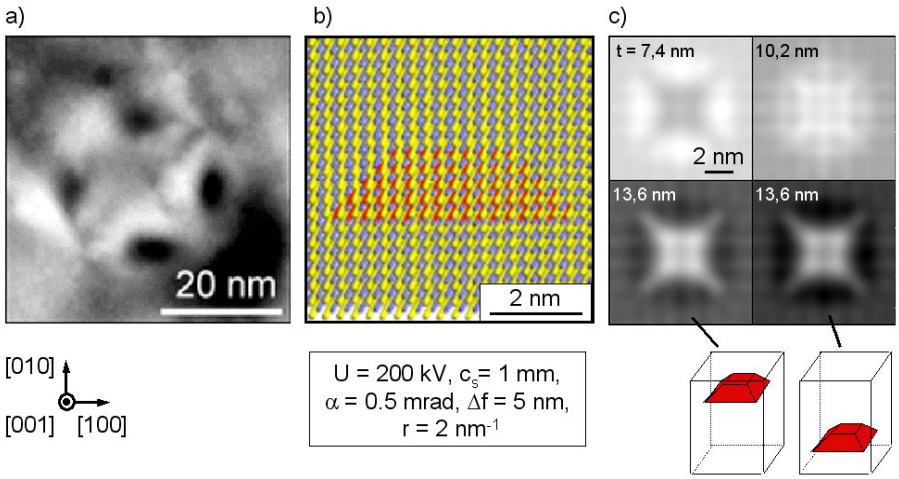

Fig. 6: Simulation of diffraction contrast feature of a CdSe QD in plan view;
a) experimental image, b) structurally relaxed super cell,
c) simulated features for several thicknesses.

In correspondence to the fourfold symmetry of the contrast feature the QD was assumed by the simulations to exhibit tetragonal symmetry as well. Inside four supercells the following CdSe pyramids were defined: (1) complete and (2) truncated CdSe pyramid having {101} facets with the edges of the basal plane oriented parallel ⟨100⟩ and 5 nm long. In addition, (3) a complete and (4) a

truncated CdSe pyramid having {111} facets with the edges of the basal plane oriented parallel ⟨110⟩ were created. In order to simulate the structural properties of the strained system CdSe/ZnSe each supercell structure was recalculated by means of molecular dynamics structure relaxation based on a rescaled empirical Stillinger-Weber potential (Ruvimov [6]).

In Fig. 6b the structurally relaxed supercell is partially drawn. Inside of it the truncated CdSe pyramid having {101} facets is seen. For all supercells image contrast simulations were done by using the EMS software (Stadelmann [7]). The parameters for the calculations were chosen with respect to the experiment as given in Fig. 6 with U – acceleration voltage, c_S – spherical aberration, α – beam-semiconvergence, Δf – defocus spread, and r – aperture size. The images were calculated with a defocus value of $\Delta = 25$ nm lying between the Gauss and the Scherzer focus. The thicknesses values chosen for the calculation of series are t = 7.4 nm, 10.2 nm, and 13.6 nm. For the latter case two positions of the pyramid inside the supercell were assumed as depicted in the lower part of Fig. 6c.

The results of the contrast simulations shown in Fig. 6c exhibit the best agreement with the experimental findings in comparison to the other three assumptions (Scheerschmidt [8]). Therefore, the CdSe QDs can be visualized as truncated pyramids with the edges of the basal plane aligned parallel to the ⟨100⟩ directions and exhibiting {110} facets (Kirmse [9]). This orientation is in contrast to that found for QD pyramids of III-V materials. One explanation of this difference might be the higher ionicity of CdSe in comparison to, e.g., (In,Ga)As making the non-polar {110} facets more favourable than the polar {111} ones, i.e. neutral surfaces are predominantly expected to form contrary to charged ones for reasons of minimization of the surface energy.

The location of the pyramids within the supercell (near the entrance or the exit surface with respect to the electron beam) does not remarkably influence the contrast, probably because of the small slab thicknesses. However, one should be aware that the contrast is very sensitive to the sample thickness. Always a dark-bright contrast reversal could be obtained in between the minimum and maximum thickness chosen in the simulations.

3.2. Ga(Sb,As) QUANTUM DOTS ON (In,Ga)As SEED QUANTUM DOTS

The semiconductor system Ga(Sb,As)/GaAs performs self-organized formation of QDs via Stranski-Krastanov growth mode due to the lattice mismatch of about 7 % between GaSb and GaAs. The finally formed Ga(Sb,As) QDs have a size of only some nanometres in diameter. For any application of QDs their chemical and physical properties have to be as homogeneous as possible. The formation of a regular lateral arrangement of Ga(Sb,As) QDs with a sufficiently narrow size distribution is hardly to achieve [10]. In order to overcome this problem a seed layer of InAs QDs capped with a GaAs layer is deposited prior to the Ga(Sb,As) growth providing an array of favourable positions for the formation of the Ga(Sb,As) QDs [11]. The samples were grown by metal-organic vapour phase deposition at a growth temperature of 470°C ([12], [13]).

TEM investigations of these structures mainly aimed at the determination of structural properties like size, shape, and strain driven vertical correlation of the QDs but also on the chemical composition.

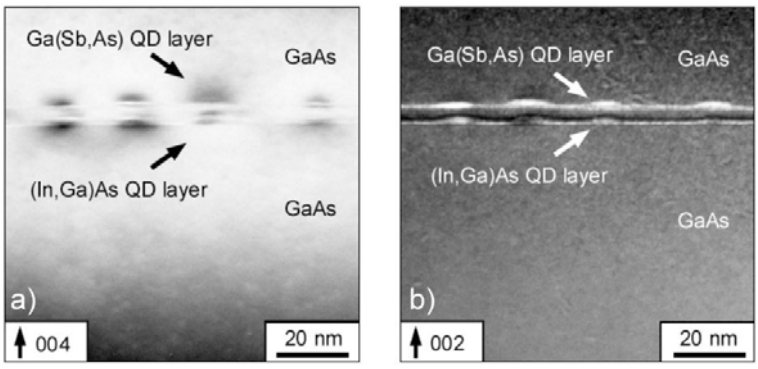

Fig. 7: Dark-field imaging of Ga(Sb,As) QDs on (In,Ga)As seed QDs;
a) strain-sensitive 004 dark-field image and b) chemically sensitive 002 dark-field image.

In Fig. 7 an instructive example is presented of the different contributions of strain and chemical composition to the dark-field image contrast.

The 004 dark-field image of Fig. 7a provides information on the extension of the strain field of the individual (In,Ga)As QD at one hand into the underlying GaAs substrate but also into the GaAs above. From the direct vertical correlation of the QDs as seen in Fig. 7a it has to be concluded that the strain field has reached up to that surface onto which the Ga(Sb,As) was deposited.

The 002 dark-field image of Fig. 7b shows exactly the same region as Fig. 7a. The narrow bright lines represent the (In,Ga)As and the Ga(Sb,As) wetting layer, respectively, which is broadened at points where the QDs are located. For (In,Ga)As the bright regions are accompanied by two dark lines above and underneath indicating regions where the composition of $In_xGa_{1-x}As$ is between $0 \leq x \leq 0.4$ (Rosenauer [14]). For these values the intensity of the 002 beam is smaller than that of GaAs presuming constant thickness of the sample. Compared to GaAs the higher brightness of the inner line of (In,Ga)As wetting layer and seed QDs denotes that the maximum In content is significantly higher than 0.4. Contrary to that, the Ga(Sb,As) QD layer shows a gradual change of the brightness without any intermediate minimum. This gives a monotonic dependence of the amplitude of the 002 beam on the Sb content in the system Ga(Sb,As). The lateral size of the Ga(Sb,As) QDs derived from their cross sections amounts to 10 to 15 nm. The height is about 2 to 3 nm giving an aspect ratio of width over height of 5. The QDs were found free of defects as derived from diffraction contrast imaging as well as from high-resolution TEM. Hence, the high lattice mismatch is purely elastically relaxed to a certain amount by the formation of QDs on top of a wetting layer.

Summarizing this chapter it can be stated that from diffraction contrast images of both projections – plan view and cross section – a number of information on the QDs properties can be derived, as, e.g., on their area density, lateral and vertical arrangement, lateral size, height, defect behaviour, presence of a wetting layer and, when a chemically sensitive reflection is present, also on the chemical composition.

4. PHASE CONTRAST IMAGING

In order to get an insight of the structure and composition of the QDs even on an atomic scale HRTEM has to be applied. In order to do this the specimen has to be oriented with a low indexed zone axis (usually [110] or [100]) parallel to the direction of the incident beam (cf. Fig. 8).

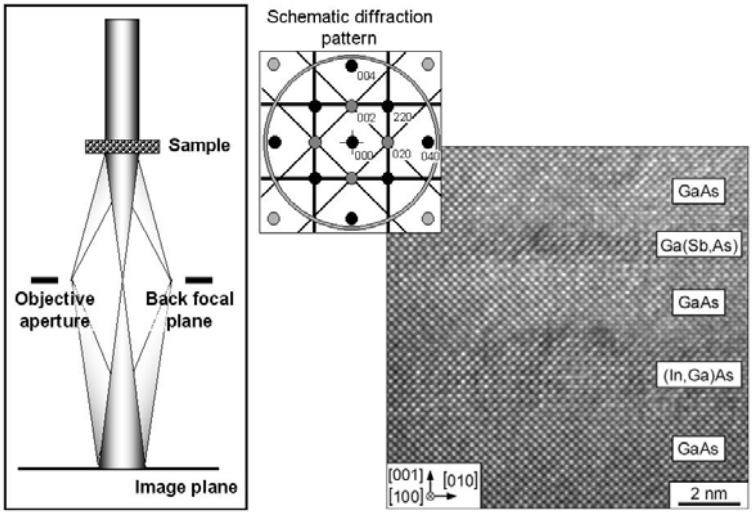

Fig. 8: High-resolution TEM imaging; schematic ray path, corresponding diffraction pattern, and representative atomically resolved image

For this alignment a number of beams are excited which can be selected by an appropriate large objective aperture. At the image plane the beams interfere and generate the image of the atomic structure as seen in the right part of Fig. 8 for a Ga(Sb,As) QD vertically correlated to an (In,Ga)As seed QD. The image was recorded at a c_S–corrected microscope where delocalization phenomena are eliminated ensuring the imaging of interfaces without broadening.

In general, the direct interpretation of an HRTEM image is not possible due to the complexity of both the scattering and the imaging process. Therefore, the image simulation and the trial-and-error matching techniques are the indirect way of structure retrieval, see e.g. [15]. The other possibility of structure retrieval is the determination of the scattered wave function at the exit surface of the crystalline specimen by electron holography or focus series reconstruction techniques ([16], [17]). The possibilities of the retrieval of the object information by solving inverse problems in electron diffraction are outlined in [18].

5. QUANTITATIVE HRTEM

In this chapter it will be discussed how a special technique of qHRTEM can be used to determine structural peculiarities on atomic scale of Ga(Sb,As) QDs.

In the last decade various methods have been developed to extract quantitative information on the atomic structure, the elastic strain and the chemical composition from high-resolution TEM micrographs. A very comprehensive review on the different methods and program packages of qHRTEM is given by Kret et al. [19].

One of these packages is the DALI software developed by Rosenauer et al. [20]. DALI stands for digital analysis of lattice images.

The flowchart of the analysis is given in Fig. 9. The aim of this analysis is to determine the distribution of a selected lattice distance and concluding from that to evaluate the composition of the island material.

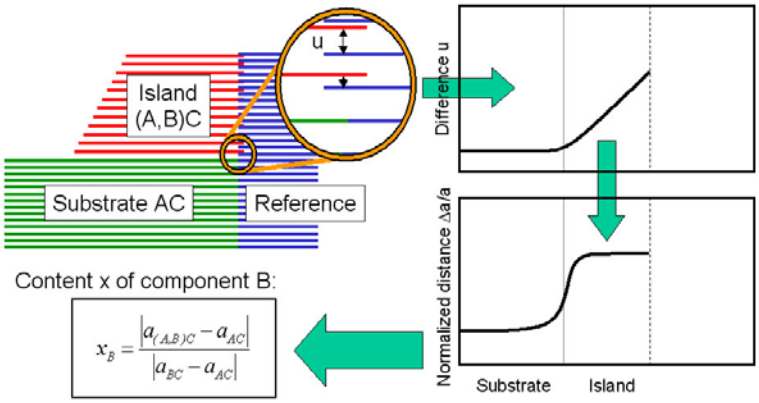

Fig. 9: Extraction of information on composition from lattice distance analysis of high-resolution TEM images.

Let us assume an island of the ternary compound (A,B)C grown on a binary substrate AC. The island material has a larger vertical lattice distance compared to the substrate. In order to detect the distribution of the lattice distance a reference lattice (given in blue) is defined at a non-strained region of the substrate. The reference lattice (RL) is extended to the whole area of interest. Consecutively, the difference $\boldsymbol{u}$ is measured between the lattice distance of the inspected region and that of the RL. The normalized derivative of $\boldsymbol{u}$ gives the distribution of the vertical lattice distance. In the last step the content of the component B in the ternary compound is calculated applying Vegards rule. Strictly speaking, this rule holds for bulk crystals only. When applying to a TEM specimen one has to take into account that thin foil relaxation takes place. For applicability of the rule the t/λ criterion has to be

fulfilled [21]. Since the thickness of the region imaged in the right part of Fig. 8 is not known the following analysis is restricted to the determination of the distance of the 002 lattice planes.

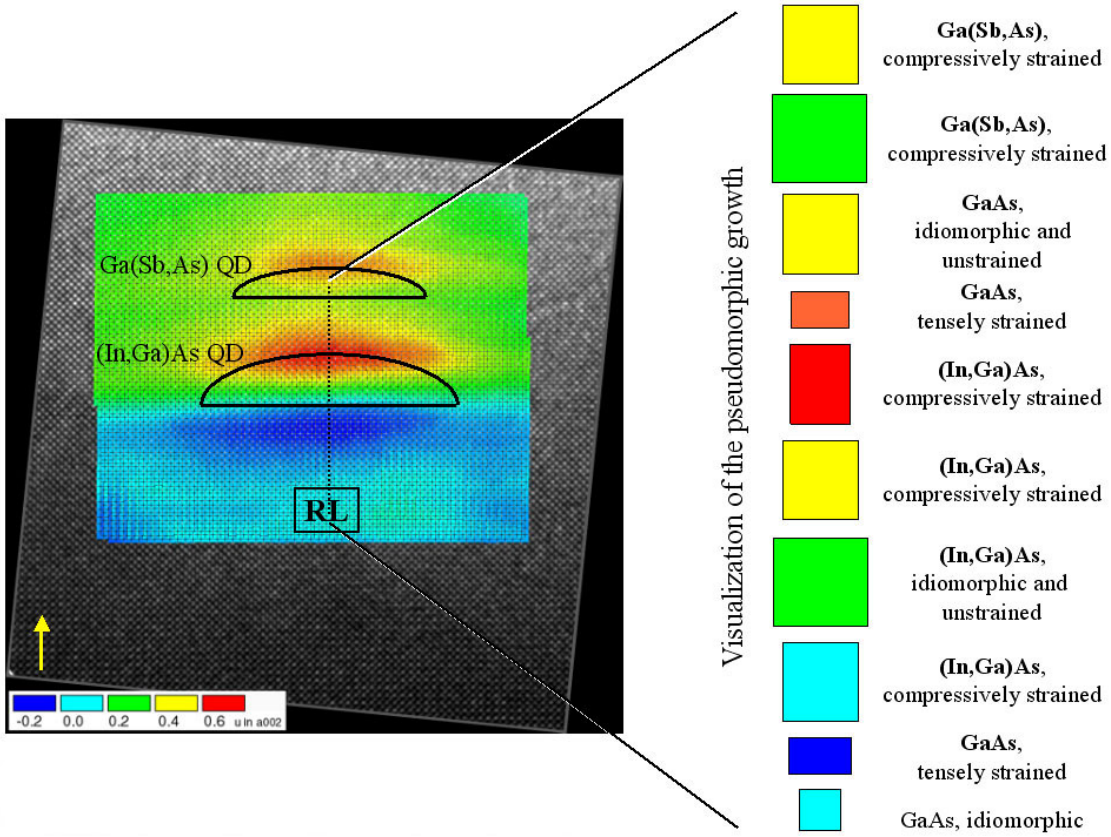

Fig. 10: Strain analysis of 002 lattice planes of stacked Ga(Sb,As) QD on (In,Ga)As seed QD

In Fig. 10 the results of the quantitative analysis of an HRTEM image are given [22]. The strain distribution is shown as a colour-coded map. The indicator of the strain is the displacement. For the region where the RL is defined (given in light blue) the mean displacement is zero. Approaching the (In,Ga)As QD the colour changes to dark blue. This symbolizes that the lattice distance of GaAs parallel to [001] is smaller than that of the RL. The (In,Ga)As QD induces a strain into the GaAs substrate by increasing the lateral distance of the nearest neighbours. Since its volume has to remain the unit cell is shrunken in growth direction. The rectangles symbolize the projection of the unit cell perpendicular to the electron beam. From the width of the rectangles also the thin foil relaxation is recognizable.

Going ahead along the [001] direction and focusing on the QD area the colour changes from blue to green after only two 002 planes. The beginning of this steep gradient marks the lower border of the (In,Ga)As QD [23]. Green, subsequently yellow, and finally red indicate the increase of $\boldsymbol{u}$ due to replacement of Ga by In causing a larger volume of the unit cell. The maximum of $\boldsymbol{u}$ is reached at the centre of the red area coinciding with the top of the (In,Ga)As QD. The height of the QD concluded from this analysis amounts to about 1.3 nm.

Within the GaAs spacer layer the displacement $\boldsymbol{u}$ decreases to a minimum given as a mixture of yellow and green. Assuming the same lattice plane distance of GaAs like in the RL the value of $\boldsymbol{u}$ has to remain constant. But, $\boldsymbol{u}$ decreases which is an indication for a strained GaAs unit cell with smaller lattice distance parallel [001] compared to the RL. Approaching the lower interface of the upper QD $\boldsymbol{u}$ increases again due to the larger lattice distance of Ga(Sb,As) compared to GaAs. The maximum of $\boldsymbol{u}$ is given in orange. The height of the Ga(Sb,As) QD is about 0.9 nm.

In the region above the two QDs and beside $\boldsymbol{u}$ shows nearly homogeneous values being associated with unstrained GaAs of homogeneous composition. The different colours (blue and green) of the

adjacent GaAs is caused by the (In,Ga)As wetting layer. The influence of the Ga(Sb,As) wetting layer on ***u*** is not detected by this analysis.

6. ANALYTICAL TEM

Analytical TEM is performed for the investigation of QD composition and of diffusion and segregation phenomena in the region of the QDs. The TEM methods available for this purpose become more and more sophisticated benefiting from both the development of the microscopes and the computer assistance.

Beside the energy-filtered TEM (EFTEM) and STEM / Z contrast method discussed in this paper a number of other methods can give some information on the composition of the area investigated. As discussed in the previous chapters TEM dark-field imaging using a chemical sensitive reflection and corresponding simulation of the intensity of the beam is a potential method. A number of methods of qHRTEM is used for determination of composition, as, e.g., CELFA (composition evaluation by lattice fringe analysis [24]), exit wave reconstruction [17], and the combined application of HRTEM imaging and image contrast simulation. The well established method of energy dispersive X-ray spectroscopy (EDXS) (see, e.g., [2] and [25]) has the advantage to be sensitive to elements having a larger atomic number. Applying the different STEM modes, i.e., point analysis, line scan, and elemental map comprehensive compositional information on the specimen can be gained. Disadvantage of EDXS is the poor energy resolution being about 100 eV. In some cases this hinders the detection of elements exhibiting similar energies of its ionisation edge. By using electron energy loss spectroscopy (EELS) it is possible to overcome the problem of poor energy resolution. Processes of inelastic interaction between specimen and incoming electrons, e.g., excitation of an X-ray quantum, causes an energy loss of the transmitted electrons. Hence, the EELS signal is complementary to the EDXS signal. Depending on the limitations of the EEL spectrometer the energy interval is limited between 0 eV and 3 keV. The energy resolution is defined by the electron source. For a thermal LaB_6 cathode the energy resolution is about 1 to 2 eV, whereas for a field emission gun (FEG) an energy resolution below 1 eV is achievable. In principle the same STEM modes are used for EELS as for EDXS (i.e. point analysis, and line scan). For imaging of 2-dimensional distribution of the elements the method of energy-filtered TEM is available.

6.1. Energy-filtered TEM

The technique of energy-filtered TEM (EFTEM) is applied in imaging mode using two main constructive approaches for an energy filter. In order to equip an existing microscope the post-column filter (Gatan Imaging Filter – GIF) can be attached. The alternative approach is the in-column filter being incorporated in the microscope column between intermediate lens system and projective lens system.

In an energy-filtered image the 2-dimensional distribution is visualized of all electrons which suffered the same energy loss. After a background detection, simulation and subsequent subtraction the elemental signal is given. The most established procedure for obtaining an elemental map is the three-window technique. Here, two pre-edge images and one post-edge image are acquired. Using the two pre-edge images the background image is extrapolated for subtraction from the post-edge image.

One example of an elemental map is shown in Fig. 11a for a single (In,Ga)As QD in a GaAs matrix. The map was required by using the Ga-M_{23} ionization edge having an energy of $\Delta E = 103$ eV. The distribution of Ga exhibits a minimum at the region of the QD caused by partial replacement of Ga by In. The (In,Ga)As wetting layer which is a clear evidence for the Stranski-Krastanov growth mode can be easily recognized in the map as well. Some inhomogeneity inside the QD region hints to an additional elastic scattering process undergone by the inelastic scattered electrons. One confirmation of this assumption is the presence of lattice planes in the Fourier filtered image (see Fig. 11b). This can be interpreted as an artefact of the analysis within the low-loss region up to 100 eV. In Fig. 11c two grey scale scans are given showing the vertical extension of both the QD

(about 3 nm) and the wetting layer (about 1 nm). Especially the profile across the wetting layer shows the high spatial resolution of the method of about 1 nm.

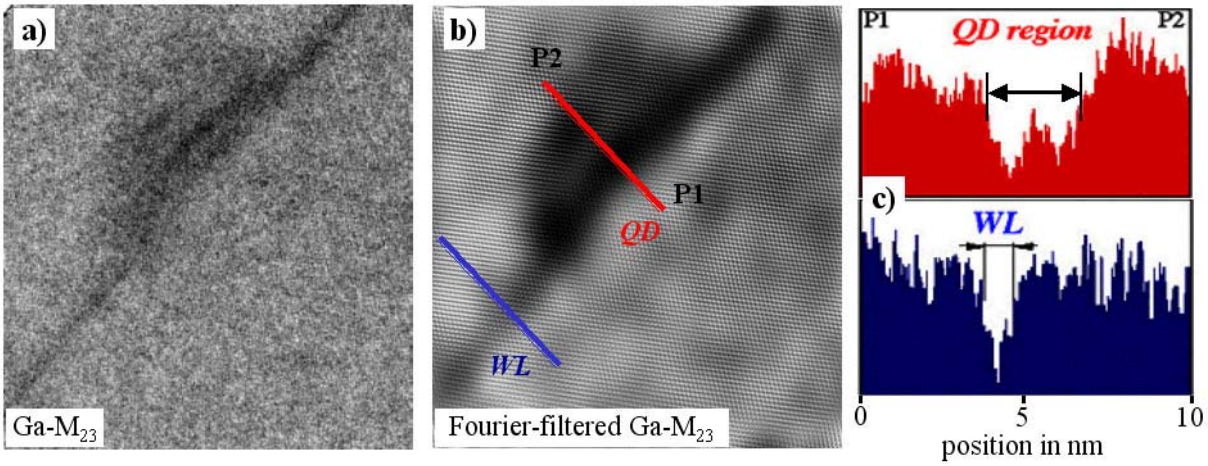

Fig. 11: Energy filtered TEM of an individual (In,Ga)As QD;
a) Ga map, b) Fourier filtered image, c) grey scale scans across QD and wetting layer (WL).

The elemental map solely gives a qualitative information on the distribution of an element. With respect to the interpretation of the elemental maps it has to be noticed that artifacts can arise both from inhomogeneous specimen thickness and from contributions of elastically scattered electrons.

EEL spectroscopy provides some quantitative information via simulation of spectra when the cross section of each element is known. Moreover, the sample thickness has to be small enough to fulfill the criterion that the intensity of the first plasmon peak is about 1/10 of the intensity of the zero loss peak.

6.2. STEM / Z contrast imaging

Z contrast method utilizes the scattering process which the incident electrons undergo while passing the specimen. One result of this process is the angular distribution of the transmitted electrons. The scattering angle depends on the mean atomic number Z of the specimen material. For higher Z the scattering angle is larger (cf. Fig. 12).

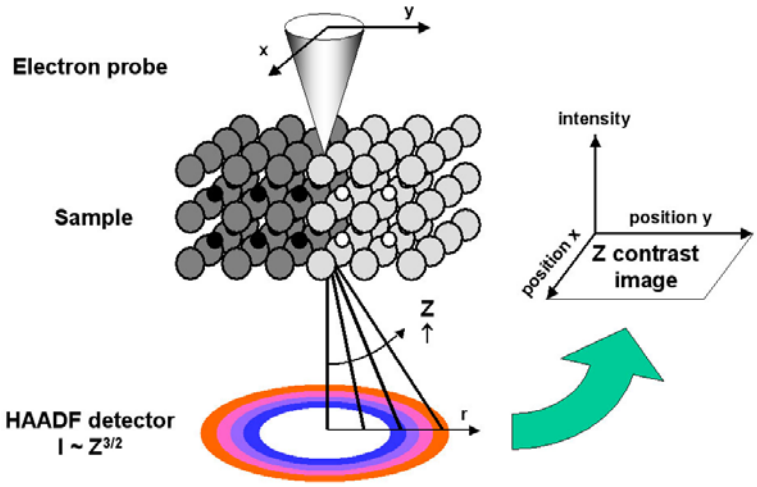

Fig. 12: Image formation of STEM / Z contrast method.

Z contrast imaging is realized in STEM mode by scanning the electron beam across the sample. The angular distribution is detected by an high-angle annular dark-field (HAADF) detector. Due to the geometry of the detector the signal at the detector is proportional to $Z^{3/2}$. The Z contrast image is produced by plotting the registered intensity with respect to the actual beam position. Atomically resolved images can be realized when the diameter of the electron probe is as small as the interatomic distance, i.e., smaller than 0.3 nm.

The STEM / Z contrast method was applied to the double QD structure of Ga(Sb,As) on (In,Ga)As [26]. In the left part of Fig. 13 the resulting image is given. Higher image intensity represents material of higher mean atomic number. Hence, the lower bright region corresponds to the (In,Ga)As QD, whereas the upper bright stripe represents the Ga(Sb,As) QD. In order to better visualize the QDs a line scan from A to B of the image intensity is drawn. Perpendicular to the line AB the intensity is averaged within the area marked by the blue rectangle. Both QDs are clearly seen in the line scan as intensity maxima above the background marked by the dashed line. The decrease of the background approaching position B is due to decreasing sample thickness.

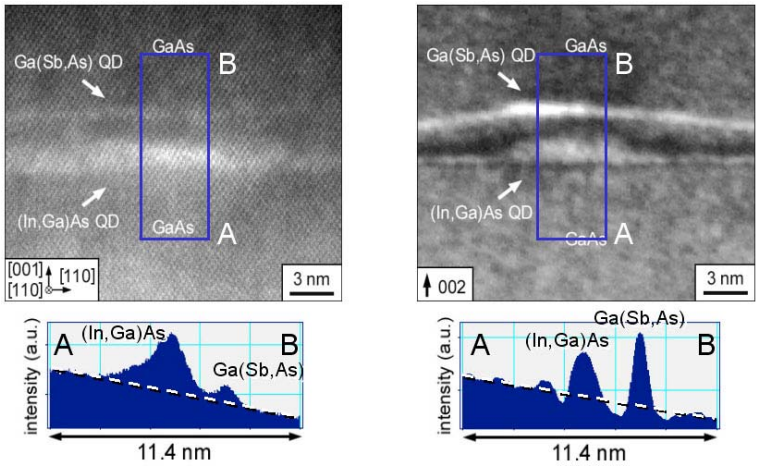

Fig. 13: Comparison of chemically sensitive imaging methods:
left) STEM Z contrast, right) 002 dark-field diffraction contrast

The results of Z contrast measurements can be compared with other chemically sensitive methods. In the right part of Fig. 13 an 002 dark-field image is presented of one and the same TEM specimen.

As already shown in chapter 3 the intensity of the 002 beam shows a minimum for (In,Ga)As at a In content of about 25 % instead of Ga. Hence, there is no direct correlation of intensity in the image and the content. The intensity profile given in the lower right part of Fig. 13 reveals a local minimum underneath and above the Ga(Sb,As) QD as well.

In conclusion, STEM / Z contrast imaging provides a direct information on the chemical composition.

7. LIMITATIONS OF INVESTIGATION OF QUANTUM DOT STRUCTURES

In general, results of TEM investigations can only be interpreted with respect to the limitations of the individual TEM method.

Compared to an epitaxial sample of an initial lateral size of 10 mm x 10 mm the area for TEM investigations is extremely restricted. Depending on using plan-view or cross-section specimen the area inspected is usually smaller than some 100 μm^2 (plan view) or even less than 1 μm^2 (cross section). If the conditions of epitaxial growth are not constant all over the sample the results gained for a limited area can not be representative for the whole sample. For more reliable results more than one

TEM specimen of the sample have to be examined. Lateral inhomogeneous sample properties also affect the comparability of results for plan-view and cross-sectional projection.

Specimen preparation is a second limitation of TEM due to being a destructive method. Most of the material of initial sample has to be removed for a specimen transmittable for electrons. This process causes numerous artefacts. The optimization of TEM specimen preparation with respect to minimization of structural defects was already discussed in chapter 2.

A further restriction is thin-foil relaxation. The self-organized formation of QDs is a strain-induced process. Hence, inside the epitaxial sample a certain amount of strain energy is stored. When the strained material is thinned down to some 10 nm it undergoes a relaxation process. The comparison between the geometry of unit cells of a strained bulk sample and a TEM specimen is given in Fig. 14.

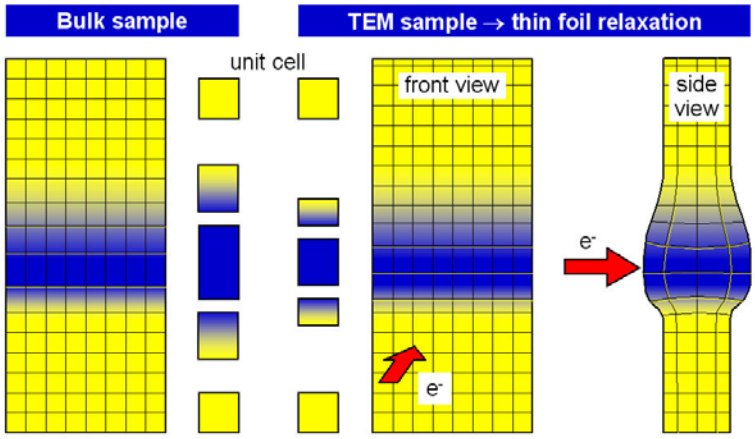

Fig. 14: Thin-foil relaxation of TEM sample due to strain.

Let us assume a bulk sample containing a compressively strained layer (given in blue) inside a matrix (yellow). For minimization of strain energy pure elastic relaxation is supposed. In-plane relaxation is impossible because of the adjacent layer material compressed as well. Thus, relaxation of strain can only be realized into growth direction. The corresponding geometry of the unit cells shows an enlargement solely of its vertical size. Here, the vertical measure of the unit cell is directly correlated to the strain and even to the composition. Vegards rule can be applied (cf. Fig. 9).

Contrary to that, in-plane relaxation is possible in a TEM specimen perpendicular to the foil plane (see "side view" in Fig. 14). For this case the vertical size of the unit cell can be smaller than that of the unstrained matrix. A direct correlation between vertical lattice distance and the composition does not longer exist. Nevertheless, the determination of the composition of layer or QD is possible by applying finite element calculation. Thin-foil relaxation can be simulated when the foil thickness and the elastic parameters of the strained materials are known. Iterative optimization of agreement between calculated strain distribution and the one obtained in the experiment by varying the composition parameter of the layer or the QD respectively yields the composition itself.

A last artefact discussed here of the TEM investigations of QDs is the matrix effect for the determination of the composition via any chemically sensitive method. At one hand, the size of QDs ranges between a few nanometres up to some ten nanometres. On the other hand, the sample thickness can amount from 10 nm up to about 100 nm. One have to be aware of not only analyzing the single QD but in addition the surrounding matrix as schematically drawn in Fig. 15. Although analizing a uniformly composed QD a concentration profile can be received which justifies an inhomogeneous elemental distribution due to the geometry of the QD inside the matrix. In order to bypass this artefact it is necessary to determine both the specimen thickness and the lateral size of the individual QD. In a first approximation the same size of the QD can be assumed of its basal plane viewed parallel to the electron beam. An analysis of only the QD is ensured when the specimen thickness is about the lateral size of the QD.

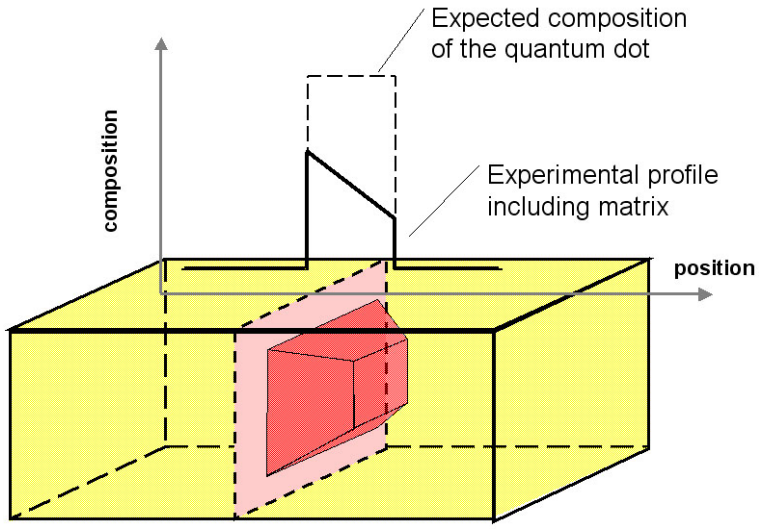

Fig. 15: Matrix effect for determination of composition of QDs.

Although there are a number of artefacts strongly affecting the interpretation it is important to get all the information attainable by the various TEM methods. The big advantage of TEM is that for an individual QD a number of independent results can be received at a lateral resolution of about 1 nm.

8. SUMMARY

QDs of compound semiconductors have a size of only some nanometres in all the spatial directions. Thus, the structural and chemical characterization of QDs requires methods having an appropriate spatial resolution. TEM fulfils this requirement. Due to the strong interaction of the incident electrons with the specimen an appropriate strategy for thinning down to a thickness of less than 100 nm has to be applied affecting the properties of the initial sample as little as possible.

For the investigation of structural and chemical peculiarities of the QDs a number of methods can be performed. Due to the presence of both chemically and strain-sensitive reflections diffraction contrast imaging in dark-field mode delivers information on the chemical composition as well as on several structural parameters as, e.g., size, shape, area density, and vertical and lateral correlation.

High-resolution TEM is applied for structural investigation on an atomic scale. The strain distribution inside and in the adjacency of the QDs is subsequently evaluated by means of quantitative HRTEM. Here, a digital image analysis is performed of the interdistance of the lattice planes. The corresponding results can be understood when considering thin-foil relaxation.

Chemically sensitive TEM methods, i.e., energy-filtered TEM, STEM / Z contrast imaging, and to some extend also 002 dark-field imaging provide qualitative information on the composition of the QDs. Matrix effect has to be taken into account when quantifying of chemical composition.

The numerous modes of TEM give comprehensive data on structural and chemical properties of the QDs. The results delivered by TEM are indispensable for understanding the self-organized formation as well as the electronic and optical properties of the semiconductor QDs.

ACKNOWLEDGEMENT

The epitaxialy grown QD samples were provided by Prof. F. Henneberger (HU Berlin, CdSe/ZnSe) and by Prof. D. Bimberg (TU Berlin, III-V QDs). TEM specimen preparation was carried out by E. Oehlschlegel. Molecular dynamics calculation of CdSe/ZnSe supercells were done by Dr. K. Scheerschmidt and Dr. D. Conrad (MPI Halle). Prof. K. Urban is gratefully acknowledged for provision of c_S-corrected microscope at Ernst-Ruska Centre at Research Center Juelich and

Dr. M. Lentzen for kind assistance at the microscope. Thanks are due to Dr. R. Schneider (now MLU Halle) for providing the EFTEM results. STEM / Z contrast imaging was performed by Dr. Kawasaki (JEOL).

REFERENCES

[1] D. Bimberg, M. Grundmann, N.N. Ledentsev, Quantum dot heterostructures, John Wiley & Sons, Chichester, 1998.

[2] D.B. Williams, C.B. Carter, Transmission Electron Microscopy: A Textbook in Materials Science, Plenum Press, New York, 1996.

[3] P.G. Goodhew, Thin foil preparation for electron microscopy, in: Practical methods in electron microscopy, M. Glauert (Ed.), Elsevier, New York (1985).

[4] A. Barna, in Specimen preparation for transmission electron microscopy of materials – III, R. Anderson, B. Tracy, J. Bravman (Eds.), Mat. Res. Symp. Proc. 254 (1992) 3.

[5] H. Kirmse, R. Schneider, R. Rabe, W. Neumann, and F. Henneberger, Appl. Phys. Lett. 72 (1998) 1329

[6] S. Rouvimov and K. Scheerschmidt, Phys. Status Solidi (a) 150 (1995) 471.

[7] P. A. Stadelmann, Ultramicroscopy 21 (1987) 131.

[8] K. Scheerschmidt, D. Conrad, H. Kirmse, R. Schneider, and W. Neumann: Electron microscope characterization of CdSe/ZnSe quantum dots based on Molecular Dynamics Structure Relaxations, Ultramicroscopy 81 (2000) 289.

[9] H. Kirmse, R. Schneider, K. Scheerschmidt, D. Conrad, and W. Neumann, J. Microsc., 194 (1999) 183.

[10] L. Müller-Kirsch, R. Heitz, U. W. Pohl, D. Bimberg U. W. Pohl, D. Bimberg, Appl. Phys. Lett., 79 (2001) 1027.

[11] G. Medeiros-Ribeiro, R. L. Maltez, A. A. Bernussi, D. Ugarte W. d. Carvalho, J. Appl. Phys., 89 (2001) 6548.

[12] L. Müller-Kirsch, U. W. Pohl, R. Heitz , H. Kirmse, W. Neumann, D. Bimberg, J. Cryst. Growth, 221 (2000) 611.

[13] L. Müller-Kirsch, R. Heitz, A. Schliwa, O. Stier, D. Bimberg, Appl. Phys. Lett., 78 (2001) 1418.

[14] A. Rosenauer, U. Fischer, D. Gerthsen, A. Förster, Ultramicroscopy 72 (1998) 121.

[15] G. Möbus, R. Schweinfest, T. Gemming, T. Wagner, M. Rühle, J. Microscopy, 190 (1998) 109.

[16] H. Lichte, M. Lehmann, Adv. in Imaging and Electr. Physics, 123 (2002) 225.

[17] A. Thust, W. M. J. Coene, M. Op de Beeck, D. van Dyck, Ultramicroscopy, 64 (1996) 211.

[18] K. Scheerschmidt, J. Microscopy 190 (1998) 238.

[19] S. Kret, P. Ruterana, A. Rosenauer, D. Gerthsen, phys. stat. sol (b), 227 (2001) 247.

[20] A. Rosenauer, S. Kaiser, T. Reisinger, J. Zweck, W. Gebhardt, D. Gerthsen, Optik 101 (1996) 1.

[21] M.M.J. Treacy, J.M. Gibson, J. Vac. Sci. Technol. B4 (1986) 1458.

[22] R. Otto, H. Kirmse, I. Häusler, W. Neumann, A. Rosenauer, L. Müller-Kirsch, D. Bimberg, Appl. Phys. Lett., 85 (2004) 4908.

[23] W. Neumann, H. Kirmse, I. Häusler, R. Otto, I. Hähnert, Journal of Alloys and Compounds 382 (2004) 2.

[24] A. Rosenauer, U. Fischer, D. Gerthsen, A. Förster, Ultramicroscopy 72 (1998) 121.

[25] D. Shindo, T. Oikawa, Analytical Electron Microscopy for Materials Science, Springer-Verlag, Tokyo, 2002.

[26] W. Neumann, Materials Chemistry and Physics 81 (2003) 364.